Mendeleev Commun., 2027, **37**, Just accepted

Mendeleev Communications

26/8163

Received 30.07.26
Revised 09.10.26

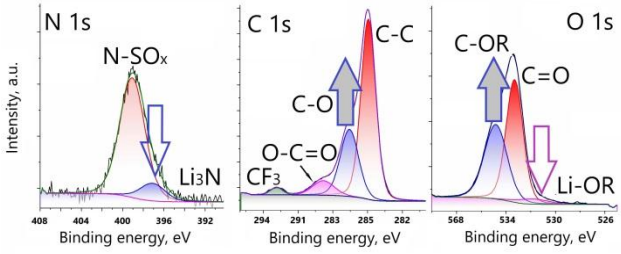
Lithium anode surface modified by *in situ* polymerization of oligomers with diacrylate groups

Alena V. Yudina,[a] Anna A. Slesarenko,[a] Galiya Z. Tulibaeva,[a] Evgeny N. Kabachkov,[a,b] Yuriy I. Baluda,[a] Alexander V. Mumyatov[a] and Olga V. Yarmolenko*[a]

[a] *Federal Research Center of Problems of Chemical Physics and Medicinal Chemistry, Russian Academy of Sciences, 142432 Chernogolovka, Moscow Region, Russian Federation. E- mail: oyarm@icp.ac.ru*
[b] *Yu. A. Osipyan Institute of Solid State Physics, Russian Academy of Sciences, 142432 Chernogolovka, Moscow Region, Russian Federation*

DOI: 10.71267/mencom.8163

An additive for liquid electrolyte based on polyethylene glycol diacrylate (PEGDA) has been developed. PEGDA (5-10 wt.%) in 1 M LiTFSI in diglyme polymerizes in situ during cell cycling on the surface of metallic lithium, as confirmed by XPS and FTIR spectroscopy. The polymer protection ensured stable cycling of lithium-polyimide batteries at 100°C during 150 charges - discharge cycles.



XPS spectra of the lithium surface before and after cycling

Keywords: liquid electrolyte, LiTFSI, diglyme, polyethylene glycol diacrylate, Li//polyimide cell, SEI.

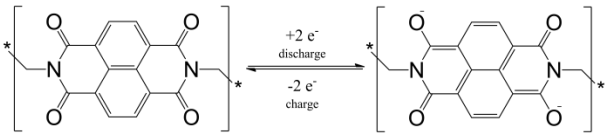
Lithium metal is considered an ideal material for next-generation battery anodes.[1,2] When combined with high-capacity organic cathodes, lithium metal batteries (LMB) provide high energy density.[3,4] However, problems such as dendrite growth and the formation of inactive lithium lead to reduced cycling stability and lead to safety risks. To solve the problems of the lithium anode surface, different approaches are used to form a protective layer (solid electrolyte interphase) SEI.[5-8]

To improve the safety of LMB, an additive based on polyethylene glycol diacrylate (PEGDA) was developed, which can crosslink at the terminal double bonds and form a network polymer when initiated by benzoyl peroxide.[9] However, it is known that C=C bonds can also open when attacked by an electron, as, for example, in vinylene carbonate.[10-12] Thus, in this work, the concept of electron-induced polymerization of a small molecule was applied to an oligomer with a higher molecular weight.

In the work, a liquid electrolyte (LE) based on the composition of 1 M solution of $LiN(SO_2CF_3)_2$ in diglyme (G2) was used, with the addition of PEGDA oligomer in the amount of 5 and 10 wt.% of molecular weight 575 (Pol-1) and 700 (Pol-2). Structure of the PEGDA with units (—CH_2CH_2O—) is shown in Figure S1.

Dissolving the oligomer in LE yielded the initial polymerizable composition, which was placed in a cell between lithium and polyimide (PI) electrodes. The polyimide was synthesized using the method described in detail in work.[13] The composition of the cathode was developed in the work.[14]

The Li/PI cells were studied using CV analysis. A redox reaction of the PI polyimide was observed, resulting in a two-electron transition with a theoretical capacity of 203 mAh g^{-1} (Scheme 1).



Scheme 1. The two-electron redox reaction of PI polyimide.

Figure 1 (a-b) shows the CVs for the second cycle of Li//PI cells with liquid electrolytes without additives and with PEGDA additives. It is evident that in the initial liquid electrolyte, the cathodic and anodic peaks are more reversible, while in the presence of PEGDA they are not due to slower diffusion.

Figure 1 (c-d) shows the charge-discharge profiles of Li//PI cells at 100°C for cycle 15.

A comparison of the charge-discharge profiles for 15 cycles shows that the capacity of the cell with LE at 100°C reaches 150 mAh g^{-1}, while the cell with the oligomer additive achieves 160–170 mAh g^{-1}. It should be noted that adding 10 wt.% Pol-2 results in a higher irreversible capacity, presumably due to further cross-linking of the PEGDA.

Resource tests of lithium-polyimide battery prototypes were conducted over 200 cycles at 25°C and 150 cycles at 100°C at a current density of 40 mA g^{-1} (C/5) in the potential range of 1.5–3.5 V (Fig. 2).

© Mendeleev Communications.

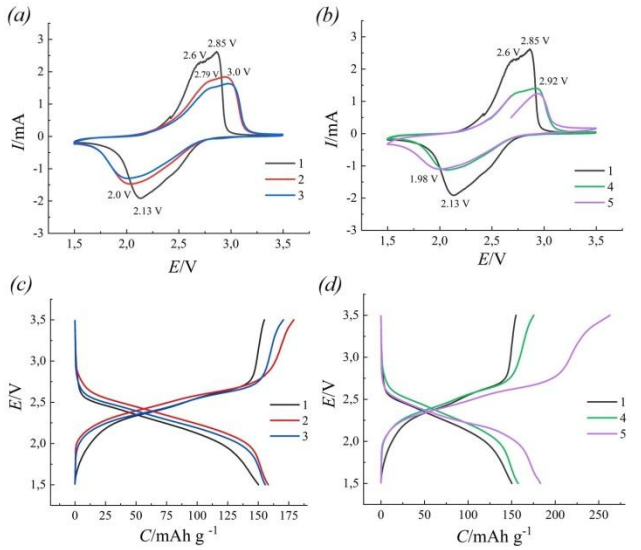


Figure 1 CV of Li//PI cells with electrolytes at a potential scan rate of 2 mVs^{-1} *(a-b)* and charge-discharge profiles at current rate C/5 in voltage range 1.5-3.5 V *(c-d)*: *(1)* LE; *(2)* LE + 5% Pol-1, *(3)* LE + 10% Pol-1; *(4)* LE + 5% Pol-2, *(5)* LE + 10% Pol-2

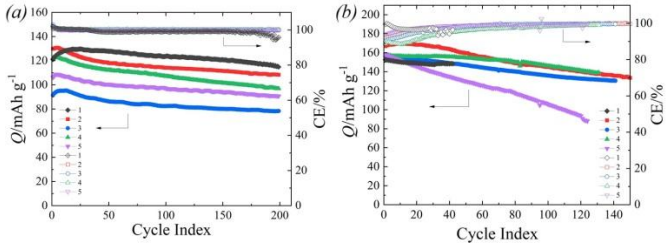


Figure 2 Dependence of discharge capacity (Filled markers) and Coulomb efficiency (Hollow markers) on the cycle number of Li//PI cells at 25 ˚C *(a)* and 100 ˚C *(b)* at current rate C/5: *(1)* LE; *(2)* LE + 5% Pol-1, *(3)* LE + 10% Pol-1; *(4)* LE + 5% Pol-2, *(5)* LE + 10% Pol-2

Figure 2 shows that at 100°C, cell capacity increases by 25% to 40% (for a cell with 10 wt.% Pol-1). Cells with LE at room temperature exhibit a maximum capacity of up to 130 mAh g^{-1}, but at 100°C, these cells short-circuited at the ~50th charge-discharge cycle (apparently due to lithium dendrites growing through the fibrous separator). This behavior was also reproduced in other cells of this composition, also at the 50th charge-discharge cycle.

Figure 2b shows that the Li//PI cell with LE containing 5 wt.% Pol-1 exhibits the highest capacity of 170 mAh g^{-1} compared to the other compositions. The cell containing 10 wt.% Pol-2 exhibits the worst performance. Apparently, a very dense polymer network forms on the surface, which impedes lithium cation diffusion at the lithium/electrolyte interface.

All Li/PI cells were studied using electrochemical impedance spectroscopy with staircase potential sweep after cycling at 100°C. This method shows the change in cell impedance during the following processes: 1) PI reduction (lithiation) and 2) PI oxidation (delithiation). In this process, the reaction $Li^+ + e \leftrightarrow Li^0$ occurs on lithium. During the first process, lithium dissolves, while during the second, it precipitates.

The Nyquist plots for Li/LE/PI cells (Figure S2) demonstrate that the LE electrolyte has undergone significant degradation. On the contrary, the Nyquist plots for Li//PI cells with oligomeric additives (Figure S3) show that the cell is operational.

It was not possible to find an equivalent circuit for the Nyquist plots of the Li/LE/PI cell, as a nonequilibrium process is observed in the first high-frequency region. Therefore, only the low-frequency region of the impedance spectrum could be accurately estimated. The Nyquist plots of the remaining cells (Figure S3) had a standard semicircle shape with an equivalent circuit describing them (Figure S4). For these cells, the dominant resistance is the polymer coating on the PEGDA lithium surface. Therefore, other interphases and processes are not visible against this maximum resistance.

The calculated equivalent circuit parameters of the Li/PI cell for electrolytes of all compositions are presented in Table S2. The data obtained in Table S2 show that LE decomposed during cycling. Its resistance is approximately 250 Ohms•cm^2. In other cases, the electrolyte resistance clearly depends on the amount of PEGDA added: the lower the amount and the lower the molecular weight, the lower the resistance of the polymer layer.

After testing, the cells were disassembled, and the lithium surfaces were examined. Optical photographs of lithium from cells after cycling, compared to the initial state are shown in Figure S5. The lithium surface from the cell with liquid electrolyte has darkened, while the surface from the cell with oligomer additives is unaffected.

The lithium surface was studied using XPS and FTIR spectroscopy. These spectra for the lithium surface from cells with liquid and oligomer-containing electrolytes showed significant differences, while the surfaces of lithium from oligomer-containing electrolytes were virtually identical. Therefore, the spectra for the composition with 5 wt.% Pol-1, which demonstrated superior electrochemical properties, will be presented below.

High-resolution XPS spectra of various elements of the lithium surface after cycling with liquid electrolyte without and with oligomer additive are shown in Figure 3.

Figure 3a shows that the SEI (solid electrolyte interface) contains compounds derived from the decomposition of LiTFSI salt, diglyme solvent, and their reduction products with lithium. These compounds include inorganic compounds (Li_2O, LiF, Li_3N, Li_2S), polymeric carbon compounds, alkoxide (ROLi), and fluorinated carbon compounds.

Figure 3b shows that the presence of the polymer decreases the content of lithium compounds (Li_3N, fluorinated carbon compounds with Li-F bonds, Li-OR alkoxides) and increases the proportion of polymer groups, including those from the oligomer. Thus, it can be concluded that the polymer covers the lithium surface, thereby preventing the decomposition of LiTFSI salt.

The FTIR spectra of the lithium surface are shown in Figure S6. It is clear from Figure S6 that the spectra of the lithium surface from electrolytes without and with the addition of the oligomer differ significantly. The main peak at 1061–1064 cm^{-1} is attributed to the O═S═O vibration of the LiTFSI salt group. The assignment of the peaks is given in Table S3, with references to the literature.[15–20]

For clarity, Figure 4 shows the 1350–1800 cm^{-1} regions for the FTIR spectra of both lithium surfaces in comparison with the oligomer and polymer-containing electrolyte.

From Fig. 4 it can be seen that the initial solution of the oligomer-containing electrolyte has similar peaks as those of the oligomer, namely, the peaks of the carbonyl group C=O in the region of 1722–1725 cm^{-1}, the peak of the C=C group in the region of 1654–1621 cm^{-1}, the peak of the C–C bond in the region of 1408–1410 cm^{-1} and the peak of the CH_2 bond (C–H) at 1456 cm^{-1}.

© Mendeleev Communications.

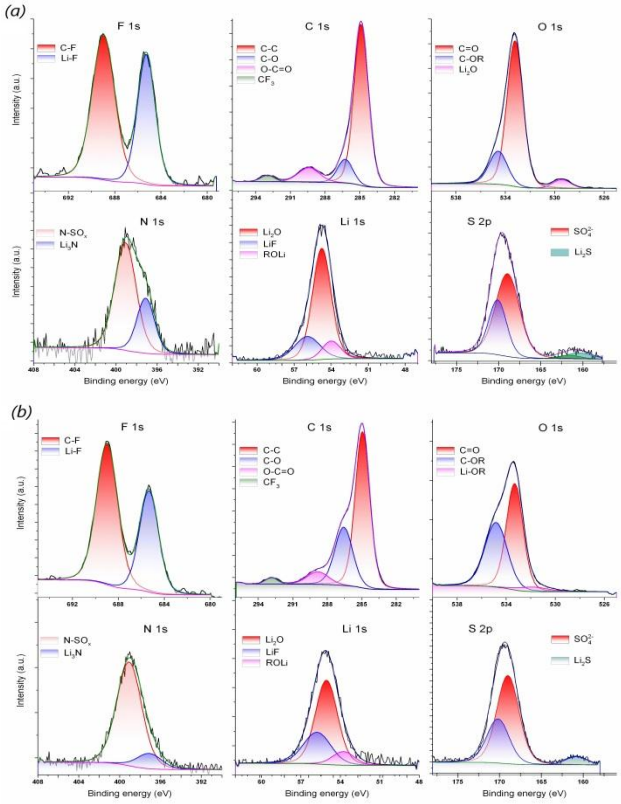


Figure 3 High-resolution XPS spectra of various elements of the lithium surface after cycling with liquid electrolyte without *(a)* and with oligomer additive *(b)*

The remaining peaks (see Table S3) can be attributed to the decomposition products of the solvent (Scheme S1) and LiTFSI salt (Scheme S2). Scheme S2 shows that under electron-rich conditions, TFSI- decomposes into reactive intermediates. These are chemically unstable, and their further decomposition leads to the formation of inorganic products of the SEI layer, such as LiF, Li_3N, Li_2O and Li_xS.

The decomposition scheme of LiTFSI salt is consistent with the literature data,[21] where the authors also showed that the O═S═O vibration peak shifts from 1057 cm^{-1} (for the initial liquid electrolyte) to 1061-1064 cm^{-1} due to the coordination of the Li+ cation with oxygen atoms without breaking the O═S═O bond.[22] This coordination draws electron density, making sulfur more electropositive and lengthening the S═O double bond, which leads to a higher vibration frequency. In addition, the authors of this work showed using the operando FTIR method that inorganic SEI (based on LiF, Li_3N and Li_2O) is not static, but exhibits dynamic evolution during cycling. Therefore, it is necessary to create a more stable polymer-based coating that does not change after its formation.

Thus, a polymerizable additive for liquid electrolyte based on oligomers with diacrylate groups was studied using a model system (1 M LiTFSI solution in diglyme). The optimal amount of oligomer for lithium protection was found to be no more than 5 wt.%. Resource testing of the Li//PI battery demonstrated a high, stable capacity of up to 160 mAh g^{-1} (per cathode active mass) at 100°C.)

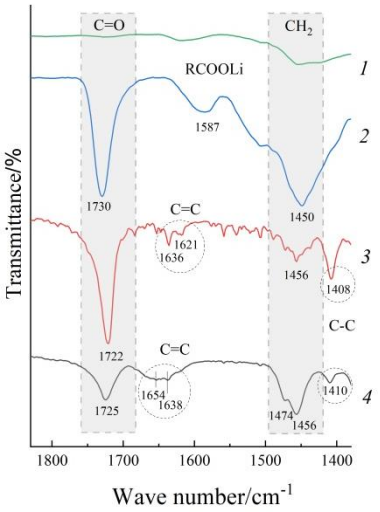


Figure 4 FTIR spectra, where: 1 - lithium surface after testing in a cell with a liquid electrolyte, 2 - lithium surface after testing in a cell with a oligomer-containing electrolyte, 3 - PEGDA oligomer, 4 - oligomer-containing electrolyte

FUNDING. The work was financial supported by the Ministry of Science and Higher Education of the Russian Federation, Project No. 075-15-2024-532.

ACKNOWLEDGMENTS. The work was partially fulfilled using the equipment of the Multi-User Analytical Center of FRC PCP MC RAS and Multi-User Center of Institute of Solid-State Physics RAS (project no. 124013000692-4).

Online Supplementary Materials

Supplementary data associated with this article can be found in the online version at doi: 10.71267/mencom.8163.

References

1 J. Liu, Z. Bao, Y. Cui, E. J. Dufek, J. B. Goodenough, P. Khalifah, Q. Li, B. Y. Liaw, P. Liu, A. Manthiram, Y. S. Meng, V. R. Subramanian, M. F. Toney, V. V. Viswanathan, M. S. Whittingham, J. Xiao, W. Xu, J. Yang, X.-Q. Yang and J.-G. Zhang, *Nat. Energy*, 2019, **4**, 180; https://doi.org/10.1038/s41560-019-0338-x

2 B. Liu, J. - G. Zhang and W. Xu, *Joule*, 2018, **2,** 833; https://doi.org/10.1016/j.joule.2018.03.008.

3 O. V. Yarmolenko, G. R. Baymuratova, G. Z. Tulibaeva, A. V. Yudina, I. K. Yakushchenko and A. F. Shestakov, *Russ. J. Gen. Chem.*, 2024, **94,** 1580; https://doi.org/10.1134/S1070363224060410.

4 A. Andezai, J.O. Iroh, *Energies*, 2025, **18**, 582. https://doi.org/10.3390/en18030582.

5 M. S. Johnson, Jr. D. Farina, L. Kavalsky, J. Zádor, R. H. West, V. Viswanathan, W. H. Green. *J. Phys. Chem. C.* 2025, ***129*** (28), 12667; https://doi.org/10.1021/acs.jpcc.5c00507

6 Y. Tanaka, T. Kawase, K. Matsuda, H. Kondo, T. Inagaki, M. Nagaoka. *J. Phys. Chem. C*, 2024, ***128*** (32), 13529; https://doi.org/10.1021/acs.jpcc.4c00099.

7 N. Takenaka, T. Fujie, A. Bouibes, Y. Yamada, A. Yamada, M. Nagaoka, *J. Phys. Chem. C*, 2018, ***122*** (5) , 2564; https://doi.org/10.1021/acs.jpcc.7b11650

8 G. Gourdin, J. Collins, D. Zheng, M. Foster, D. Qu, *J. Phys. Chem .C*, 2014, ***118*** (31), 17383; https://doi.org/10.1021/jp504181b

9 A. V. Yudina, M. P. Berezin, G. R. Baymuratova, N. I. Shuvalova and O. V. Yarmolenko, *Russ. Chem. Bulletin*, 2017, **66,** 1278; https://doi.org/10.1007/s11172-017-1885-6.

10 J. Wagner-Henke, D. Kuai, P. B. Balbuena and U. Krewer, *Energy Storage Mater.*, 2025, **81,** 104434; https://doi.org/10.1016/j.ensm.2025.104434.

11 F. Fasulo, A. B. Muñoz-García, A. Massaro, O. Crescenzi, C. Huang and M. Pavone, *J. Mater. Chem. A*, 2023,**11**, 5660; https://doi.org/10.1039/D2TA08772C.

© Mendeleev Communications.

12 Q. T. N. Phan, J. Kawamura and K. Kurihara, *Phys. Chem. Chem. Phys.*, 2022, **24,** 25611; https://doi.org/10.1039/D2CP02421G.
13 O. V. Yarmolenko, O. E. Romanyuk, A. A. Slesarenko, G. R. Baymuratova, N. I. Shuvalova, A. V. Mumyatov, P. A. Troshin and A. F. Shestakov, *Russ. J. Electrochem.*, 2019, **55,** 254; https://doi.org/10.1134/S1023193519020174.
14 A. V. Yudina, G. R. Baymuratova, A. V. Mumyatov, G. Z. Tulibaeva, E. N. Kabachkov, P. A. Troshin, A. F. Shestakov, O. V. Yarmolenko, *Mendeleev Commun*., 2022, **32**, 655; https://doi.org/10.1016/j.mencom.2022.09.029.
15 A. V. Yudina, G. R. Baymuratova, G. Z. Tulibaeva, A. L. Litvinov, A. F. Shestakov and O. V. Yarmolenko, *Russ. Chem. Bulletin*, 2020, **69**, 1455; https://doi.org/10.1007/s11172-020-2923-3
16 E. Pretsch, P. Biihlmann, C. Affolter, *Structure Determination of Organic Compounds*, Springer-Verlag, Berlin Heidelberg, 2000; 421 p.; https://doi.org/10.1007/978-3-662-04201-4.
17 W. Kam, C.-W.Liew, J. Y. Lim, and S. Ramesh, *Ionics*, 2014, **20**, 665; https://doi.org/10.1007/s11581-013-1012-0.
18 L. Wu, J. Hu, S. Chen, S. Yang, X. Liu, L. Foord, J. S. Foord, P. Pobedinskas, K. Haenen, H. Hou and J. Yang, *Electrochim. Acta*, *2023*, **466**, 142973; https://doi.org/10.1016/j.electacta.2023.142973.
19 D. Aurbach, E. Pollak, R. Elazari, G. Salitra, C. S. Kelley, and J. Affinito, *J Electrochem. Society*, 2009, **156**, A694; https://doi.org/10.1149/1.3148721.
20 Q. Rey, P. Johansson, J. Lindgren, J. C. Lassègues, J. Grondin, and L. Servant, *J Phys. Chem. A*, 1998, **102**, 3249; https://doi.org/10.1021/jp980375v.
21 S. Rahman, R. Pereira, J. Nedsaengtip and V. Kalra. *Adv. Sci*., 2026, **13,** e23503; https://doi.org/10.1002/advs.202523503.
22 B. N. Olana, S. D. Lin, and B.-J. Hwang, *Electrochim. Acta*, 2022, **416,** 140266; https://doi.org/10.1016/j.electacta.2022.140266.

Received: 30th July 2026; Com. 26/8163

© Mendeleev Communications.